AGC 226178 and NGVS 3543: Two Deceptive Dwarfs toward Virgo

Michael G. Jones[1], David J. Sand[1], Michele Bellazzini[2], Kristine Spekkens[3,4], John M. Cannon[5],
Burçin Mutlu-Pakdil[6,7], Ananthan Karunakaran[4,8], Giacomo Beccari[9], Laura Magrini[10], Giovanni Cresci[10],
John L. Inoue[5], Jackson Fuson[5], Elizabeth A. K. Adams[11,12], Giuseppina Battaglia[13,14], Paul Bennet[15],
Denija Crnojević[16], Nelson Caldwell[17], Puragra Guhathakurta[18], Martha P. Haynes[19], Ricardo R. Muñoz[20],
Anil Seth[21], Jay Strader[22], Elisa Toloba[23], and Dennis Zaritsky[1]

[1] Steward Observatory, University of Arizona, 933 North Cherry Avenue, Room N204, Tucson, AZ 85721-0065, USA; jonesmg@arizona.edu
[2] INAF–Osservatorio di Astrofisica e Scienza dello Spazio di Bologna, Via Gobetti 93/3, I-40129 Bologna, Italy
[3] Department of Physics and Space Science, Royal Military College of Canada, PO Box 17000, Station Forces Kingston, ON K7K 7B4, Canada
[4] Department of Physics, Engineering Physics and Astronomy, Queen's University, Kingston, ON K7L 3N6, Canada
[5] Department of Physics & Astronomy, Macalester College, 1600 Grand Avenue, Saint Paul, MN 55105, USA
[6] Kavli Institute for Cosmological Physics, University of Chicago, Chicago, IL 60637, USA
[7] Department of Astronomy and Astrophysics, University of Chicago, Chicago IL 60637, USA
[8] Instituto de Astrofísica de Andalucía (CSIC), Glorieta de la Astronomía, E-18008 Granada, Spain
[9] European Southern Observatory, Karl-Schwarzschild-Strasse 2, D-85748 Garching bei München, Germany
[10] INAF–Osservatorio Astrofisico di Arcetri, Largo E. Fermi 5, I-50125 Firenze, Italy
[11] ASTRON, the Netherlands Institute for Radio Astronomy, Oude Hoogeveensedijk 4,7991 PD Dwingeloo, The Netherlands
[12] Kapteyn Astronomical Institute, PO Box 800, 9700 AV Groningen, The Netherlands
[13] Instituto de Astrofísica de Canarias, Vía Láctea s/n E-38205, La Laguna, Spain
[14] Universidad de La Laguna, Avda. Astrofísico Fco. Sánchez, La Laguna, Tenerife E-38205, Spain
[15] Space Telescope Science Institute, 3700 San Martin Drive, Baltimore, MD 21218, USA
[16] University of Tampa, 401 West Kennedy Boulevard, Tampa, FL 33606, USA
[17] Center for Astrophysics, Harvard & Smithsonian, 60 Garden Street, Cambridge, MA 02138, USA
[18] UCO/Lick Observatory, University of California Santa Cruz, 1156 High Street, Santa Cruz, CA 95064, USA
[19] Cornell Center for Astrophysics and Planetary Science, Space Sciences Building, Cornell University, Ithaca, NY 14853, USA
[20] Departamento de Astronomía, Universidad de Chile, Camino El Observatorio 1515, Las Condes, Santiago, Chile
[21] Department of Physics & Astronomy, University of Utah, Salt Lake City, UT, 84112, USA
[22] Center for Data Intensive and Time Domain Astronomy, Department of Physics and Astronomy, Michigan State University, East Lansing, MI 48824, USA
[23] Department of Physics, University of the Pacific, 3601 Pacific Avenue, Stockton, CA 95211, USA

Abstract

The two sources AGC 226178 and NGVS 3543, an extremely faint, clumpy, blue stellar system and a low surface brightness dwarf spheroidal, are adjacent systems in the direction of the Virgo cluster. Both have been studied in detail previously, with it being suggested that they are unrelated normal dwarf galaxies or that NGVS 3543 recently lost its gas through ram pressure stripping and AGC 226178 formed from this stripped gas. However, with Hubble Space Telescope Advanced Camera for Surveys imaging, we demonstrate that the stellar population of NGVS 3543 is inconsistent with being at the distance of the Virgo cluster and that it is likely a foreground object at approximately 10 Mpc, whereas the stellar population of AGC 226178 is consistent with it being a very young (10–100 Myr) object in the Virgo cluster. Through a reanalysis of the original ALFALFA H I detection, we show that AGC 226178 likely formed from gas stripped from the nearby dwarf galaxy VCC 2034, a hypothesis strengthened by the high metallicity measured with MUSE VLT observations. However, it is unclear whether ram pressure or a tidal interaction is responsible for stripping the gas. Object AGC 226178 is one of at least five similar objects now known toward Virgo. These objects are all young and unlikely to remain visible for over ∼500 Myr, suggesting that they are continually produced in the cluster.

Unified Astronomy Thesaurus concepts: Low surface brightness galaxies (940); Dwarf galaxies (416); Galaxy interactions (600); Tidal tails (1701); H I line emission (690); Virgo Cluster (1772)

1. Introduction

Blind surveys of neutral hydrogen (H I) in the local universe have revealed a plethora of extremely high mass-to-light ratio systems that have few or no stars (Saul et al. 2012; Adams et al. 2013; Cannon et al. 2015). Optical and interferometric follow-up observations have demonstrated that many of these systems are likely high-velocity clouds associated with the Milky Way or routine gaseous tidal features (Bellazzini et al. 2015a;

Cannon et al. 2015; Sand et al. 2015; Adams et al. 2016; Beccari et al. 2016). However, some may be genuine Local Group dwarfs, similar to Leo T (Irwin et al. 2007) and Leo P (Giovanelli et al. 2013), while others appear to be unusual objects in the direction of the Virgo cluster (Cannon et al. 2015; Bellazzini et al. 2015b; Sand et al. 2015; Adams et al. 2015). Uncovering what this class of objects are, how they form, and how common they are is key to understanding the lowest-mass regime of the galaxy luminosity function and how stars populate the lowest-mass halos that form galaxies. This letter focuses on one such system.

The AGC 226178 and NGVS 3543 system (Figure 1, left) was first identified in the Arecibo Legacy Fast ALFA
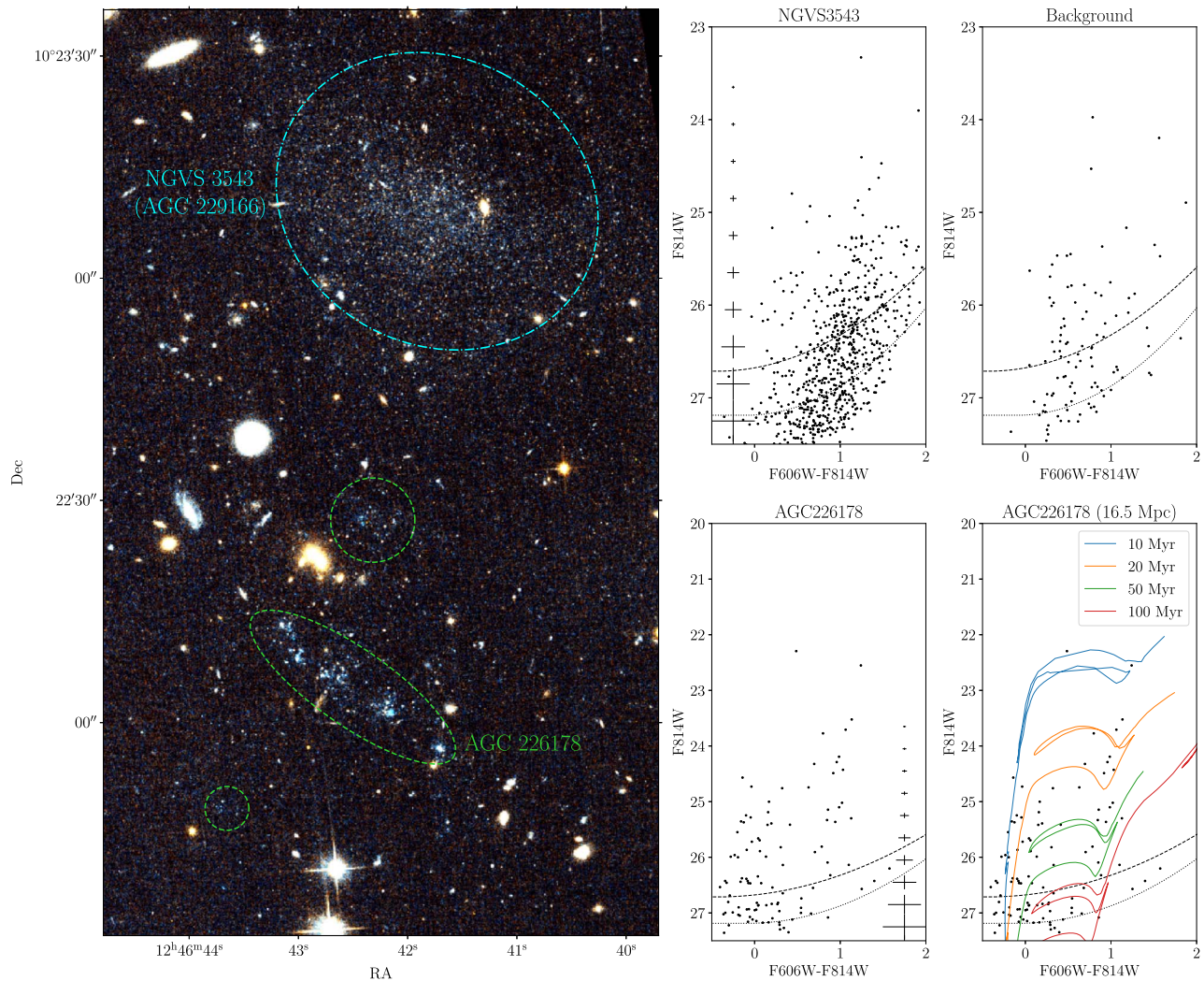
Figure 1. Left: false-color F606W+F814W image of the AGC 226178 and NGVS 3543 system. The cyan dashed–dotted ellipse encircles NGVS 3543 out to the half-light radius (Junais et al. 2021, their Table 2), and the green dashed ellipse and circles show AGC 226178. Top middle: CMD of NGVS 3543 constructed from the stars within two half-light radii (i.e., four times the area of the cyan dashed–dotted ellipse). The dashed line indicates the 90% completeness limit, and the dotted line is the 50% limit. The error bars along the edge indicate typical uncertainties in the photometry as a function of F814W magnitude. Top right: CMD of a blank sky region of equal area on the opposite side of the ACS field of view. Bottom middle: CMD of AGC 226178 constructed from the stars within the green dashed ellipse and circles. The error bars along the edge indicate typical uncertainties in the photometry. No background CMD is included; however, the area of AGC 226178 is ∼30% of NGVS 3543, and only ∼seven points in the CMD are expected to be background. Bottom right: repeated CMD of AGC 226178 with stellar population isochrones overlaid for a variety of different ages (assuming the distance to Virgo). Note that the completeness limits in the lower and upper CMDs are the same but appear different due to the different ranges of F814W magnitudes plotted.

(ALFALFA) survey (Giovanelli et al. 2005; Kent et al. 2008; Haynes et al. 2011) and followed up with the Jansky Very Large Array (VLA) to map the distribution of H I emission as part of the ALFALFA "Almost Darks" project (Cannon et al. 2015), a sample of bright extragalactic H I detections that have scarcely visible stellar counterparts. The system lies on the eastern side of the Virgo cluster, approximately 1°.4 SE of M60 and 4° SE of M87 (about 400 kpc and 1.2 Mpc in projection, respectively). Object AGC 226178 was originally identified in the ALFALFA survey as an H I–only detection with no clear optical counterpart; hence, it was included in the "Almost Darks" sample. The low surface brightness (LSB) dwarf spheroidal NGVS 3543 (cyan dashed–dotted ellipse in Figure 1) was noted at the time as a nearby object possibly related to the H I detection but too offset from the H I centroid to be the counterpart (Kent et al. 2008). The actual stellar counterpart was essentially invisible given the depth of the

Sloan Digital Sky Survey (SDSS; York et al. 2000) imaging available at the time.

The VLA observations of the H I in the system (Cannon et al. 2015) localized the emission centered on a Galaxy Evolution Explorer (GALEX; Martin et al. 2005) source approximately 1′ to the south of NGVS 3543.[24] This faint, blue, and clumpy object is visible in deeper optical imaging and highlighted in our Hubble Space Telescope (HST) image by a green dashed ellipse and circles (Figure 1, left panel). Henceforth, we refer to both this blue stellar counterpart and the H I detection as AGC 226178. Based on the SDSS and GALEX imaging available at the time, Cannon et al. (2015) settled on the interpretation that AGC 226178 is a normal, low-mass, gas-rich

---

[24] Cannon et al. (2015) referred to NGVS 3543 as AGC 229166, its original designation. However, we prefer the former to avoid confusion between NGVS 3543 (AGC 229166) and AGC 226178.

galaxy likely falling into the Virgo cluster and that NGVS 3543 is not physically connected to it.

The blue, clumpy appearance of AGC 226178 is reminiscent of another heavily studied object, SECCO 1 (Bellazzini et al. 2015b; Sand et al. 2015), also known as AGC 226067 (Adams et al. 2015). SECCO 1 was originally identified as an ultracompact high-velocity cloud (Adams et al. 2013), thought to be a candidate for a new low-mass Local Group object. If it were not for the higher recession velocity of AGC 226178 and the close proximity of NGVS 3543, then AGC 226178 might also have been classified this way. The lack of resolved stars in subsequent ground-based observations of SECCO 1 (Bellazzini et al. 2015b; Sand et al. 2015; Adams et al. 2015) and the color–magnitude diagram (CMD) from HST imaging (Sand et al. 2017) suggested that it was far beyond the Local Group, most likely in the Virgo cluster. The high metallicity of this object, given its low stellar mass, indicated that it probably formed from gas pre-enriched by a larger galaxy (Beccari et al. 2017). At present, the most likely hypothesis is that SECCO 1 formed from ram pressure or tidally stripped gas either from the group of dwarfs containing VCC 319, 322, and 334 (Bellazzini et al. 2018) or from the M86 subgroup near the cluster center (Sand et al. 2017). The similarity between SECCO 1 and AGC 226178 (and other blue star-forming clumps in Virgo) suggests that there may be many such systems in or around the Virgo cluster that have been previously missed due to their extreme properties.

Most recently, Junais et al. (2021) revisited AGC 226178 using optical, Hα, and UV data from the Next Generation Virgo cluster Survey (NGVS; Ferrarese et al. 2012), the Virgo Environmental Survey Tracing Ionised Gas Emission (Boselli et al. 2018), and the GALEX Ultraviolet Virgo Cluster Survey (Boselli et al. 2011). They came to the striking conclusion that the origin of the gas that formed AGC 226178 was NGVS 3543, which they classified as an ultradiffuse galaxy (UDG; a very LSB galaxy with the stellar mass of a dwarf but a half-light radius similar to the Milky Way; e.g., van Dokkum et al. 2015). In this scenario, both objects are assumed to be Virgo cluster members, and star formation (SF) in the UDG (NGVS 3543) would have been recently shut off when its gas reservoir was lost through ram pressure stripping by the intracluster medium (ICM). This stripped gas then underwent in situ SF, forming the stellar counterpart of AGC 226178. This hypothesis was supported by a faint UV bridge detected between the two objects and an analysis of the spectral energy distribution of NGVS 3543, which indicated that SF was only recently shut off.

In this letter, we present new HST F814W and F606W imaging with Advanced Camera for Surveys (ACS) and Multi Unit Spectroscopic Explorer (MUSE) observations with the Very Large Telescope (VLT), as well as a reanalysis of the original ALFALFA H I data and the VLA H I mapping from Cannon et al. (2015). Together, these data provide a new perspective on this system and drastically alter the interpretation of its formation mechanism.

We adopt 16.5 Mpc (Mei et al. 2007) as the distance to the Virgo cluster throughout.

2. Observations and Reduction
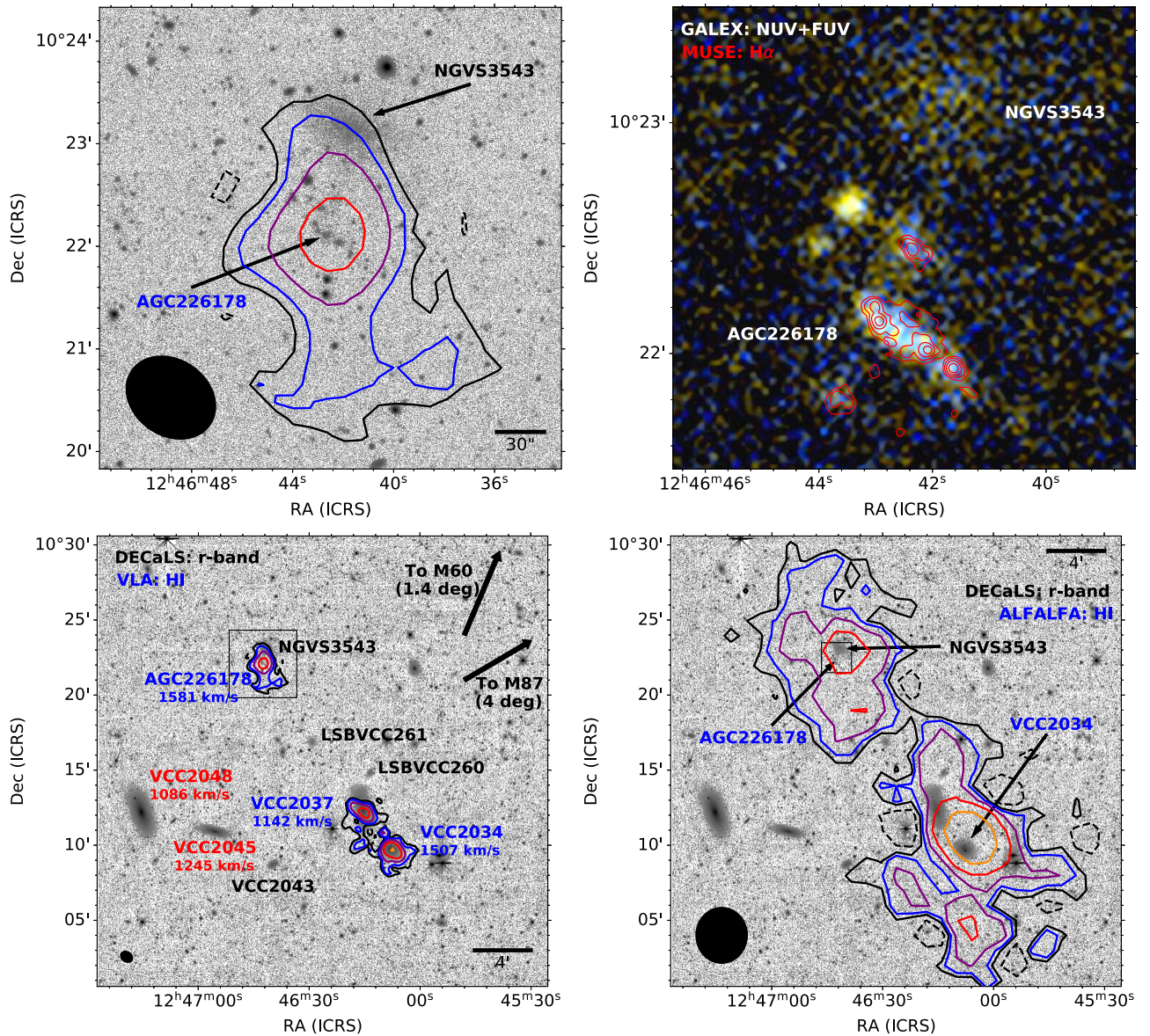
2.1. HST Observations

As part of program 15183 (PI: D. Sand), AGC 226178 was targeted with ACS in the F606W and F814W filters. The total exposure times were 2120 and 2180 s for the two filters, respectively. A combined F606W and F814W false-color image of the system is shown in Figure 1 (left). The standard ACS tools in DOLPHOT (Dolphin 2000, 2016) were used to align the individual exposures and perform photometry on all pointlike sources.[25] To select stars from the resulting DOLPHOT catalog, we selected all type 1 and 2 (pointlike) objects with magnitude uncertainties of less than 0.3 (in both filters) and no photometry flags. We set a crowding limit of 1 mag in the two filters combined and enforced a combined absolute sharpness value of less than $\sqrt{0.075}$ and a roundness threshold of less than 1 in both filters. Galactic extinction corrections (Schlafly & Finkbeiner 2011) were made based on the dust maps of Schlegel et al. (1998) at the position of each star. The typical $E(B - V)$ value was 0.024 mag for both objects.

The completeness limit of each combined field was estimated using artificial star tests in DOLPHOT. We generated 2×10^5 artificial stars with F606W magnitudes ranging from 21 to 30 and F606W – F814W colors in the range $-1 <$ (F606W – F814W) <2. These were randomly placed over the image and extracted as if real stars. They were then split into color bins, and the recovery fraction as a function of F814W magnitude was fit with an error function. The measured limits (from the error function shape parameters) for 50% and 90% recovery fractions were then fit with the combination of a horizontal line and a one-sided parabola (e.g., Figure 1, middle panels). At (F606W – F814W) = 1 mag, the F814W 90% and 50% completeness limits are 26.4 and 26.9 mag, respectively.

2.2. VLA Observations

Object AGC 226178 was observed previously as part of the ALFALFA "Almost Darks" sample (Cannon et al. 2015) and rereduced for this work. Standard calibration and reduction methods were applied using the Common Astronomy Software Applications (CASA) package (McMullin et al. 2007). However, this rereduction used an improved automatic masking of sources during the tclean task. A full description of the data reduction pipeline will be presented in Inoue et al. (in preparation). These data have a channel width of 7.81 kHz ($\sim$1.65 km s^{-1}) and a total bandwidth of 8 MHz. The final imaging used Briggs's robust = 0.5 weighting to provide a compromise between sensitivity and angular resolution for the detected H I emission. The resulting beam size was 56″ × 45″. During imaging, the channels were averaged and rebinned to a velocity resolution of 5 km s^{-1}. The resulting rms noise in 5 km s^{-1} channels is 1.2 mJy beam^{-1}. The source mask for AGC 226178 was generated with the Source Finding Application (SoFiA; Serra et al. 2014, 2015). SoFiA's main algorithm adds pixels to a mask based on a signal-to-noise ratio (S/N) threshold after smoothing to various resolutions both spatially and in velocity. We applied a 3.5σ threshold after smoothing with spatial Gaussian kernels with widths of

---

[25] DOLPHOT was run with the following parameters: FitSky = 1, RAper = 4, Force1 = 0, Align = 4, AlignIter = 3, ACSuseCTE = 1, and standard values of all other parameters.

Figure 2. Top left: contours of integrated H I emission (moment zero map) from the VLA observations of AGC 226178 overlaid on a DECaLS *g*-band image. The contour levels are -3σ, 3σ, 6σ, 12σ, 24σ, and 48σ, where 3σ corresponds to 1.6×10^{19} cm^{-2} or, equivalently, 0.13 $M_\odot$ pc^{-2} (both over 20 km s^{-1}). The beam is shown by the black ellipse in the bottom left corner ($56'' \times 45''$). Top right: GALEX NUV+FUV composite image showing a smaller field of view containing AGC 226178 and NGVS 3543. The red contours show Hα emission mapped by MUSE (contour levels are 5, 15, 45, and 135×10^{-20} erg s^{-1} cm^{-2}). Object AGC 226178 is detected strongly in both GALEX bands and Hα; NGVS 3543 is $\sim 1'$ to the north and only weakly detected in GALEX. Bottom left: VLA H I contours overlaid on a DECaLS *r*-band image showing a wide field, including several nearby galaxies that AGC 226178 may have interacted with (contours at the same levels as in the top left panel). The thin black square shows the field of view of the top left panel. Galaxies with H I detections are labeled in blue, those without H I are in red, and those with no redshift measurement are in black. Bottom right: ALFALFA H I integrated emission contours overlaid on the same optical image. The thin black square shows the field of view of the top right panel. The significance of the contour levels is the same, but in this case, 3σ corresponds to 2.8×10^{18} cm^{-2} or, equivalently, 0.02 $M_\odot$ pc^{-2} (both over 20 km s^{-1}). The beam is shown by the black ellipse in the bottom left corner ($3'.8 \times 3'.5$). In this case, the H I emission of VCC 2037 has been excluded to avoid confusion.

approximately one and two times the beam diameter and a box kernel over 20 and 40 km s^{-1} (four and eight channels). A 90% reliability threshold was applied, which SoFiA estimates based on the apparent flux of negative (presumably spurious) sources. The resulting moment zero map is shown overlaid on a Dark Energy Camera Legacy Survey (DECaLS; Dey et al. 2019) *g*-band image in Figure 2 (top left).

2.3. MUSE/VLT Observations

Panoramic, integral-field, intermediate-resolution ($R = 2000$–4000) spectroscopy in the wavelength range

4650–9300 Å of an $\simeq 1'.0 \times 1'.0$ field centered on AGC 226178 was acquired with MUSE@VLT (Bacon et al. 2014) as part of observing program 0101.B-0376A (PI: R. Muñoz). Here we provide only an essential description of the process of data reduction and analysis following the procedures of Beccari et al. (2017); a detailed description of these procedures will be provided in a dedicated paper (M. Bellazzini et al. 2022, in preparation). Six $t_{\text{exp}} = 966$ s exposures were acquired with a dithering scheme based on regular derotator offsets to improve flat-fielding and homogeneity of the image quality across the field. The raw data were wavelength and flux

calibrated and combined into a single stacked data cube. Then we searched for individual sources with SExtractor (Bertin & Arnouts 1996) as peaks standing $\geqslant 3.0\sigma$ above the background in an Hα and white-light image[26] obtained from the stacked cube by integration in wavelength (over 4650–9300 Å). Next, we measured the aperture fluxes of the detected sources (with SExtractor, aperture radius $= 1\rlap{.}''5$) in each slice of the cube with a wavelength step of 1.25 Å. Ultimately, the fluxes of the individual slices were recombined into a 1D spectrum for each source. Visual inspection of all of the extracted spectra lead us to identify 15 sources (most of which are resolved or marginally resolved) with at least Hα in emission in the range of velocity spanned by galaxies in Virgo ($-500 < cz_\odot$ km s^{-1} < 3000; e.g., Mei et al. 2007). These sources are all coincident with the various components of AGC 226178 shown in Figure 1 (left), and all have a very similar recession velocity, with a mean $\langle cz_\odot \rangle = 1584$ km s^{-1} and a standard deviation of $\sigma = 4$ km s^{-1}.

2.4. ALFALFA Data

The ALFALFA (Giovanelli et al. 2005) observations were taken with the 305 m Arecibo telescope in Puerto Rico between 2005 and 2011. The survey adopted a two-pass drift-scan strategy, giving a total effective integration time of 48 s at any given point within the survey footprint. Radio frequency interference was semimanually identified and flagged before the drift scans were combined into cubes spanning $2\rlap{.}^\circ4 \times 2\rlap{.}^\circ4$ on the sky, with $1'$ pixels and an angular resolution of approximately $4'$. The cube containing AGC 226178 spans approximately $-2000 < cz_\odot$ km s^{-1} < 3000 with a channel width of ~ 5 km s^{-1} and velocity resolution of 10 km s^{-1} (the full survey redshift range of $-2000 < cz_\odot$ km s^{-1} $< 18{,}000$ was split into four overlapping subranges). The cube has an rms noise of 2.4 mJy channel^{-1} and a beam size of $3\rlap{.}'8 \times 3\rlap{.}'5$. Further details regarding the ALFALFA survey and its data products can be found in Haynes et al. (2011, 2018). The original detection of the H I emission of AGC 226178 was at an S/N of 10.3 and $cz_\odot = 1581$ km s^{-1}.

3. Results

3.1. HST Images and CMDs

Figure 1 shows the HST image of the AGC 226178 and NGVS 3543 system and the CMDs of the two sources. The AGC 226178 CMD contains almost exclusively blue stars, while that of NGVS 3543 is dominated by red stars. Object NGVS 3543 has a fairly smooth elliptical morphology, partially resolved into stars in the HST image, whereas AGC 226178 is decidedly clumpy and appears to be broken into multiple components. The regions (marked by green dashed lines) used to produce the CMD of AGC 226178 were manually constructed after comparison of the HST images and Hα detections in MUSE (Section 3.4). In the case of NGVS 3543 (cyan dashed–dotted ellipse), the half-light radius and axial ratio from Junais et al. (2021) were used ($r_e = 22\rlap{.}''38$, $i = 30\rlap{.}^\circ 1$, PA $= 61\rlap{.}^\circ 7$) to produce the CMD for all stars within $2r_e$ (note that the ellipse plotted only extends to $1r_e$).

In addition to the AGC 226178 CMD, in the bottom right panel of Figure 1, we overplot PARSEC (Bressan et al. 2012)

stellar isochrones for a range of ages.[27] All isochrones have a metallicity of [M/H] $= -0.39$ (Section 3.4) and the assumed distance to Virgo (16.5 Mpc). We note that, as isochrones do not depend on the initial mass function (IMF), comparing the CMD to isochrones is robust against an atypical shape of the IMF, which is a possibility for an unusual object such as AGC 226178.

The CMD is complex but reveals a young stellar population that is similar to the HST CMD of SECCO 1 (Sand et al. 2017; Beccari et al. 2017). There is a population of faint blue stars (F814W $\gtrsim 24.5$, F606W – F814W $\lesssim 0$) that are likely a combination of young main-sequence stars and slightly older blue helium-burning stars. There is also a clear sequence of stars with $23.5 \lesssim$ F814W $\lesssim 26.5$ and F606W – F814W $\gtrsim 0.6$ mag that are likely red helium-burning (RHeB) stars. There are no evident red giant branch (RGB) stars, which is to be expected if AGC 226178 is at the distance of the Virgo cluster, as the tip of the RGB (TRGB) occurs at F814W ≈ 27 at 16.5 Mpc (e.g., Rizzi et al. 2007; Jang & Lee 2017). The brightness of the RHeB stars can be used to estimate the stellar population age (e.g., McQuinn et al. 2011), with the brightest star corresponding to an age of ~ 10 Myr (at F814W $\approx$ 22.5 mag), while the faintest corresponds to an age of ~ 50 Myr. Older ages are difficult to confirm because the helium-burning branch becomes incomplete at fainter magnitudes. The age spread seen in the CMD is thus similar to that inferred from the GALEX imaging and H II region spectroscopy in the MUSE data (Sections 3.2 and 3.4).

The CMD of NGVS 3543 is discussed in detail in Section 4.3.

3.2. GALEX Star Formation Rates

Object AGC 226178 is strongly detected in both the near-UV (NUV) and far-UV (FUV) bands (Figure 2, top right) in GALEX. The total flux in each band was measured from background-subtracted GALEX tiles (GI2_125026_AGES-strip2_04 in both NUV and FUV). They were converted to magnitudes following the standard GALEX conversions (Morrissey et al. 2007) and a Galactic extinction correction based on the $E(B - V)$ values of Schlafly & Finkbeiner (2011) at the location of each source and $R_{\rm NUV} = 8.20$ and $R_{\rm FUV} = 8.24$ (Wyder et al. 2007). Assuming a distance of 16.5 Mpc for all candidates and a bolometric solar absolute magnitude of 4.74, the apparent magnitudes were converted to luminosities and, finally, to star formation rates (SFRs) following Iglesias-Páramo et al. (2006). Uncertainties in the UV fluxes and SFRs were estimated by first masking the brightest 1% of pixels in the background-subtracted GALEX tiles (to remove bright sources) and then randomly placing 10^4 circular apertures (of equal area to the aperture in question) across the entire tile in order to estimate the rms noise.

This gives the NUV flux in the combined regions of AGC 226178 as $(1.74 \pm 0.07) \times 10^{-16}$ erg s^{-1} cm^{-2} Å^{-1} and the FUV flux as $(4.02 \pm 0.09) \times 10^{-16}$ erg s^{-1} cm^{-2} Å^{-1}. These equate to SFR estimates of $\log \frac{\rm SFR_{NUV}}{\rm M_\odot\, yr^{-1}} = -3.03 \pm 0.06$ and $\log \frac{\rm SFR_{FUV}}{\rm M_\odot\, yr^{-1}} = -3.18 \pm 0.06$, respectively. The fact that these two estimates are so similar suggests that the SFR in AGC 226178 has been relatively constant over the past 100 Myr.

---

[26] The width of the point-spread function as measured on the white-light image on a bright foreground star is $\simeq 0.8''$ FWHM.

[27] http://stev.oapd.inaf.it/cgi-bin/cmd
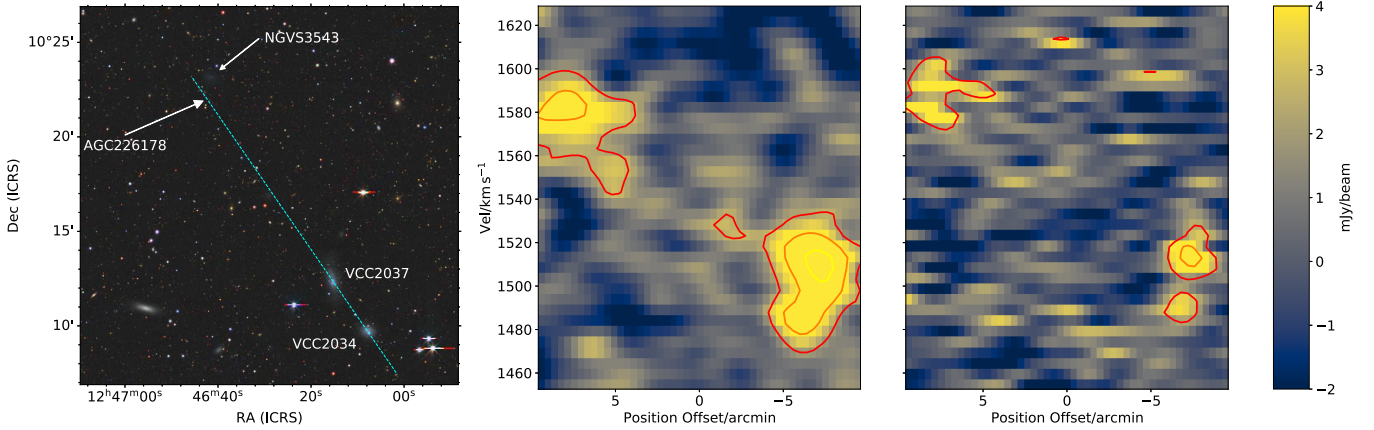
Figure 3. Left: DECaLS *grz* image showing a linear position–velocity slice (cyan dashed line) that intersects with AGC 226178 and VCC 2034. Here AGC 226178 is not visible on this scale, but its location is marked with an arrow. Middle: position–velocity slice from the ALFALFA data cube along the line in the left panel. A region 3.8′ wide (centered on the line) was collapsed to form this slice, as this corresponds to the resolution of the ALFALFA data. The contours are drawn at 2.4, 4.8, and 7.2 mJy beam^{-1}, approximately 1σ (red), 2σ (orange), and 3σ (yellow), respectively. Object AGC 226178 is the bright clump at upper left (~1580 km s^{-1}), and VCC 2034 is at lower right (~1500 km s^{-1}). Object VCC 2037 does not appear in the slice, as it is well below the velocity range plotted. Right: same position–velocity slice but from the VLA tapered data cube. A width of 1′.8 is used for the slice in this case, again roughly corresponding to the resolution of the data. For clarity, the same contour levels are used as in the middle panel; however, in this case, they correspond to approximately 1.1σ and 2.2σ.

As pointed out by Junais et al. (2021), NGVS 3543 is weakly detected in GALEX (both NUV and FUV). Making equivalent measurements (to those above) for NGVS 3543, we find an only slightly lower UV flux ($(1.18 \pm 0.19) \times 10^{-16}$ erg s^{-1} cm^{-2} Å^{-1} in NUV and $(1.47 \pm 0.24) \times 10^{-16}$ erg s^{-1} cm^{-2} Å^{-1} in FUV), though spread over a much larger area. This UV detection (particularly in FUV) would normally imply that SF has not completely ceased, as was suggested by Junais et al. (2021). However, the lack of young blue stars in the CMD (Figure 1, top middle) does not appear to agree with this interpretation. Another possibility is that blue horizontal branch stars below the completeness limit are contributing to the UV flux of this object (analogous to Yoon et al. 2004; Goudfrooij 2018). Such stars are known to exist in the old stellar populations of Local Group dwarf spheroidals (e.g., Monaco et al. 2003; Martin et al. 2017) and globular clusters (e.g., Perina et al. 2012; Dalessandro et al. 2012). However, for NGVS 3543, the color FUV − NUV = 0.58 ± 0.25, which is slightly bluer than for any of the examples above.

3.3. H I Bridge between AGC 226178 and VCC 2034

Figure 2 (top left) shows the VLA H I emission contours of AGC 226178 overlaid on a DECaLS *g*-band image. This map was constructed with SoFiA and extends to lower gas column densities than the equivalent map (based on the same observations) in Cannon et al. (2015). This deeper map reveals an extension that appears to point toward the pair of VCC galaxies, VCC 2037 ($cz_\odot = 1142$ km s^{-1}) and 2034 ($cz_\odot = 1507$ km s^{-1}), to the SW. However, no connection is evident in the VLA data (Figure 2, bottom left), even though both of these galaxies were detected in the VLA observations of AGC 226178 (about 14′ from the pointing center, where the primary beam response is at about 55%).

The total H I flux of AGC 226178 in the VLA data is 0.3 dex lower than in ALFALFA (0.31 Jy km s^{-1} compared to 0.62 Jy km s^{-1}), strongly suggesting that the VLA has missed extended or low column density emission (this was also noted as a possibility by Cannon et al. 2015). The ALFALFA

H I emission is centered at $cz_\odot = 1581$ km s^{-1}, which in this direction is consistent with the membership of Virgo (e.g., Masters 2005). Assuming a distance of 16.5 Mpc, the larger of these fluxes equates to a total H I mass of $\log M_{\rm H\,I}/M_\odot = 7.6$. Junais et al. (2021) estimated the stellar mass of AGC 266178 as $\sim 5 \times 10^4 \, M_\odot$, which means the ratio of gas to stellar mass is ~ 1000 (after multiplying the H I mass by 1.4 to account for helium). This value is exceptional, even for low-mass, gas-rich galaxies (Huang et al. 2012), indicating that AGC 226178 is not a normal low-mass galaxy.

Motivated in part by the gas inferred to be missing from the VLA observations, we returned to the original ALFALFA cube and constructed a moment zero map with SoFiA using smoothing kernels of one and two times the beam size, 0, 15, and 30 km s^{-1}, and a threshold of 3.5σ (a reliable threshold for studying extended H I streams; e.g., Taylor et al. 2020). The ALFALFA map (Figure 2, bottom right) shows an apparent H I connection between VCC 2034 and AGC 226178, resolving the question of where the latter's gas likely originated. We note here that the moment map excludes the velocity range over which there is emission from VCC 2037, so although some contours overlap with it in projection, all of the emission is actually associated with VCC 2034 and AGC 226178.

The ALFALFA data have much worse angular resolution than the VLA data; however, they also have significantly better column density sensitivity to extended emission. The majority of the additional emission in the bottom right versus bottom left panel of Figure 2 is simply below the column density sensitivity of the VLA data and would require a prohibitively long integration time to detect with the VLA (at this resolution).

To attempt to recover some of this emission in the VLA data, the data were reimaged after applying a *uv* taper of 750λ, thereby degrading the resolution of the data to about 2′.5 but improving the 3σ column density sensitivity to 3.2×10^{18} cm^{-2} (0.025 $M_\odot$ pc^{-2}) over 20 km s^{-1}, approaching the level of the ALFALFA data. In Figure 3, we show position–velocity slices for both the ALFALFA data and the tapered VLA data, covering the space between AGC 226178 and VCC 2034.

The H I emission of AGC 226178 is seen as a clump in the upper left corner of the middle and right panels of Figure 3, and VCC 2034 is the clump in the lower right corner (of either panel); VCC 2037 is well outside the velocity range plotted. The additional emission shown in the ALFALFA moment zero map (Figure 2, bottom right) appears to be made up of very low S/N features that extend from both objects toward the other (Figure 3, middle). However, when summed together over several consecutive channels to make the moment zero map, these combine to form relatively high-confidence features. These features may have formed a continuous bridge in the past or may still do so below the sensitivity of the data. The brightest part of the extension from AGC 226178 is also visible in the VLA position–velocity slice (Figure 3, right), and there may be a feature extending to lower velocities, but it is at the level of the noise. Although the quoted column density sensitivities of the two data sets now only differ by ∼25%, the ALFA beam still covers a 2.5 times larger area. Therefore, if the emission were physically spread over an area larger than the VLA synthesized beam (∼2′.5), then the effective sensitivity of the VLA data would drop significantly relative to the ALFALFA data. It is also worth noting that the two slices have different widths (see caption of Figure 3), again meaning that more extended emission could be missed by the VLA slice. Finally, the quoted column density sensitivity of the VLA data is for the pointing center (approximately the position of AGC 226178). At the location of VCC 2034, the sensitivity is approximately a factor of 2 worse.

As most of the features seen in the ALFALFA data cannot be conclusively corroborated or refuted, even with the tapered VLA data, we will primarily consider the ALFALFA data when discussing our interpretation of the system in Section 4.[28]

3.4. Velocity and Metallicity of AGC 226178 from MUSE

The MUSE observations of AGC 226178 find an abundance of clumps of Hα emission. Based on line ratio diagnostics (O III/Hβ, N II/Hα, and S II/Hα), this emission can be confidently classified as SF regions (thresholds from Kewley et al. 2001; Kniazev et al. 2008). The total Hα flux measured by MUSE is 3.13×10^{-16} erg cm^{-1} s^{-1}. This equates to a total SFR estimate of $\log \frac{SFR_{H\alpha}}{M_\odot \, yr^{-1}} = -3.09$ (converted as in Equation (2) of Kennicutt 1998), in close agreement with the UV SFR estimates. The mean heliocentric velocity of these H II regions ($cz_\odot = 1584$ km s^{-1}) also reconfirms that they are indeed associated with the H I emission.

Finally, the mean oxygen abundance was estimated by averaging over two different indicators (N2 and O3N2, adopting the calibration by Pettini & Pagel 2004) for the five sources for which it was possible to measure both indicators (as done by Bellazzini et al. 2018). These were corrected for extinction based on Hα/Hβ. The average value, ⟨12 + logO/H⟩ = 8.3 ± 0.1, supports the finding that the gas likely came from a more massive galaxy that pre-enriched it.[29] A complete analysis of the abundance measurements will be presented in a separate paper focusing on the MUSE observations (Bellazzini et al. in preparation).

---

[28] We also note that a very similar morphology is seen in the Widefield Arecibo Virgo Extragalactic Survey (Minchin et al. 2019), which is approximately twice as sensitive as ALFALFA in this region (R. Taylor, private communication).
[29] The quoted uncertainty is the standard deviation between the five sources.

Based on the stellar mass–metallicity relation (MZR) of Andrews & Martini (2013), this metallicity should correspond to a galaxy of $\log M_*/M_\odot = 8.4 \pm 0.4$. Object VCC 2034 has an i-band magnitude of 14.77 ± 0.02 and $g - i = 0.76 \pm 0.03$ (Kim et al. 2014). Using the scaling relation of Taylor et al. (2011) and assuming a distance of 16.5 Mpc gives $\log M_*/M_\odot = 8.2 \pm 0.1$ for VCC 2034, making it consistent with being the source of AGC 226178's gas.

4. Discussion

In this section, we discuss the nature of the AGC 226178 and NGVS 3543 system, focusing in particular on the formation of AGC 226178. The distribution of the H I emission seen with ALFALFA (Figure 2, bottom right) points to VCC 2034 as the origin of the gas in AGC 226178 and strongly suggests that it formed from stripped gas, making it either a tidal dwarf (TD) or the ram pressure equivalent. The elevated metallicity of the gas given the stellar mass also points to the same scenario.

Without the ALFALFA map, VCC 2034 would seem an unlikely parent galaxy because, based on its ALFALFA flux, it is only about twice as massive in H I as AGC 226178. However, as the H I emission appears to connect the two sources, and they are at almost exactly the same redshift, it is highly likely that VCC 2034 is the source of the gas. That being the case, there are still two open questions that are essential to the interpretation of this system: (1) what is the distance to the system, and (2) how was the gas stripped from VCC 2034?

4.1. Distance to AGC 226178

Given its position and velocity, the preferred distance to AGC 226178 is 16.5 Mpc, our assumed distance to objects associated with the Virgo cluster. However, without a direct distance measurement to either AGC 226178 or VCC 2034 (the apparent source of its gas), there remains the possibility that neither is genuinely in Virgo, with the second most likely distance being ∼10 Mpc (the distance to VCC 2037, based on a TRGB measurement; Karachentsev et al. 2014).

Given the morphology of the H I emission, it is reasonable to assume that AGC 226178 and VCC 2034 are at the same distance, meaning that a distance estimate to either object would constrain both. We considered estimating a Tully–Fisher relation (TFR) distance to VCC 2034; however, given its low mass, apparent low inclination, and ongoing interaction, this approach would not be reliable. In the absence of a robust distance estimate, here we note several points in favor of assuming 16.5 Mpc as the distance to this system.

1. The single strongest argument for $D \approx 16.5$ Mpc is that the numerous H II regions detected in the MUSE observations of AGC 226178 mean that it must contain very young stars (<10 Myr). When isochrones (assuming $D = 16.5$ Mpc) of various ages are overplotted on its CMD (Figure 1, bottom right), the brightest stars overlap with the 10 Myr isochrone. Moving AGC 226178 to 10 Mpc would shift this isochrone (and all others) approximately 1 mag brighter. Therefore, if AGC 226178 were at 10 Mpc, then stars of F814W ≈ 21.5 should be present in the CMD. However, there are none. As the completeness is essentially 100% at this magnitude (and the photometric errors are small), it would be difficult to explain the absence of these stars,

<div align="center">

Table 1
Properties of Galaxies in the AGC 226178 Field

</div>

Object (1)	R.A. (2)	Decl. (3)	$cz_\odot$ km s^{-1} (4)	Dist. (Mpc) (5)	g (6)	i (7)	$\log M_*/M_\odot$ (8)	$\log M_{\rm HI}/M_\odot$ (9)
AGC 226178	12:46:42.5	10:22:04.8	1581	(16.5)	19.34 ± 0.05[b]	18.50 ± 0.06[b]	~4.7[a]	7.60 ± 0.13
NGVS 3543	12:46:41.7	10:23:10.4		~10	17.50 ± 0.01[c]		6.88 ± 0.27[a]	<6.90
VCC 2034	12:46:08.1	10:09:45.9	1507	(16.5)	15.53 ± 0.02	14.77 ± 0.02	8.2 ± 0.1	7.86 ± 0.08
VCC 2037	12:46:15.3	10:12:20.0	1142	9.6 ± 1.0[d]	15.47 ± 0.02	14.54 ± 0.02	8.0 ± 0.1	7.18 ± 0.10
VCC 2045	12:46:55.5	10:10:56.7	1245	(16.5)	15.81 ± 0.02	14.72 ± 0.02	8.5 ± 0.1	<7.60
VCC 2048	12:47:15.3	10:12:12.9	1086	15.5 ± 2.0[e]	13.81 ± 0.02	12.78 ± 0.02	9.1 ± 0.1	<7.55

Notes. Columns: (1) Object name. (2) Right ascension (J2000). (3) decl. (J2000). (4) Heliocentric velocity. (5) Distance or assumed distance (if in parentheses). (6) g-band magnitude from Kim et al. ([2014](#)) unless indicated otherwise. (7) i-band magnitude from Kim et al. ([2014](#)) unless indicated otherwise. (8) Stellar mass estimate based on the g and i magnitudes and the Taylor et al. ([2011](#)) scaling relation (unless stated otherwise). Uncertainties do not include distance uncertainties. (9) H I mass measurements or limits from ALFALFA. Limits are based on the (assumed) distance of each source and the 50% completeness limit of S/N > 6.5 sources in ALFALFA (Haynes et al. [2011](#)). A velocity width of 30 km s^{-1} was assumed for NGVS 3543 and 100 km s^{-1} for VCC 2045 and 2048.
[a] Estimated by Junais et al. ([2021](#)), normalized to the relevant distance.
[b] Estimated by summing regions A, B, C, E, and H (which correspond to the clumps we identified as part of AGC 226178) from Junais et al. ([2021](#), Table 3).
[c] From Junais et al. ([2021](#), Table 2).
[d] TRGB measurement from Karachentsev et al. ([2014](#)).
[e] Globular cluster luminosity function measurement from Villegas et al. ([2010](#)). Note that there is also a TFR distance estimate (with much larger uncertainty) that places VCC 2048 behind the Virgo cluster (Theureau et al. [2007](#)).

whereas a distance of 16.5 Mpc naturally explains the observed population.

2. Object VCC 2037 is known to be at ~10 Mpc, and it is separated from VCC 2034 by approximately 350 km s^{-1}, which would be a large velocity offset if the two were part of the same foreground structure. If that were the case, then most likely, they would not be gravitationally bound to each other (as both are dwarf galaxies with $M^* \sim 10^8\ M_\odot$), and we would be seeing the system at a special time, right as they pass by each other.

3. If VCC 2034 and VCC 2037 were at the same distance, it would be likely that they would be interacting and that this interaction would be visible in H I emission, especially given the abundance of loosely bound gas in the vicinity of both galaxies. However, in both the ALFALFA and VLA data cubes, there is no clear sign of a bridge or tails extending between the two galaxies.

In light of the points above, for the remainder of the discussion, we will assume that AGC 226178 is at 16.5 Mpc, in the Virgo cluster. However, at the relevant points, we will indicate how our interpretation might change if it were actually at 10 Mpc.

4.2. Ram Pressure or Tidal Stripping?

The morphology of the integrated H I emission seen in the ALFALFA data (Figure [2](#), bottom right) indicates that the gas in AGC 226178 originated in VCC 2034, about 70 kpc to the SW (at the distance of Virgo). There are two main mechanisms by which gas is stripped in this way: tidal stripping and ram pressure stripping. The former can occur in almost any scenario where two or more galaxies (at least one of which contains neutral gas) strongly interact; the latter is only active in a region with a sufficiently dense intergalactic medium, such as a galaxy cluster. If AGC 226178 and VCC 2034 are in the Virgo cluster, then both of these mechanisms must be considered.

The one-sided morphology of the H I tail initially suggests ram pressure stripping, as these tails trail in the wake of a galaxy as it falls through the ICM and are thus one-sided. However, these tails also typically (though not exclusively;

e.g., Cramer et al. [2019](#)) point approximately radially away from the cluster center (e.g., Chung et al. [2009](#)), as galaxies usually fall toward the center. In this case, the center of the Virgo cluster is approximately NW, whereas the tail extends to the NE, almost perpendicular.

The tail is approximately 70 kpc long (in projection), and if we assume it is ~200 Myr old (i.e., at least twice as old as the oldest stars we identified), then VCC 2034 would have to have a transverse velocity of ~350 km s^{-1} for the tail to have been formed by ram pressure stripping. The mean radial velocity of Virgo cluster galaxies is 1138 km s^{-1} (Mei et al. [2007](#)), and the radial velocity of VCC 2034 is 1507 km s^{-1}, which, in this scenario, would make its total velocity relative to the cluster center about ~500 km s^{-1}. With this velocity, it would still be comfortably bound to the cluster, and the transverse velocity is small enough that it could have acquired this in the past, e.g., if it fell toward the cluster as part of a group. Therefore, ram pressure stripping is still a plausible scenario, despite the direction of the tail.

We also note that a visual inspection of the morphology of VCC 2034 in DECaLS and GALEX imaging does not appear to show a trail of stars accompanying the H I tail. This is the expected behavior of ram pressure stripping, as it acts only on the interstellar medium, whereas tidal stripping is gravitational and affects all matter equally. However, this is not conclusive, as H I gas is typically much more spatially extended (and therefore more loosely bound) than a galaxy's stellar component, meaning that H I can become heavily disturbed before any disruption of the stars is evident.

The one-sided form of the tail also does not rule out tidal stripping, as real examples of tidal stripping of H I seldom follow a simple morphology and are frequently quite one-sided (e.g., Hibbard et al. [2001](#)). The main issue with interpreting this H I tail as a tidal feature is the lack of an obvious candidate for the perturber, which we discuss in detail below.

4.2.1. Which Galaxy Could Have Stripped Gas from VCC 2034?

In this subsection, we shall assume that the gas tail formed via tidal stripping and discuss which galaxy might have been responsible.

There are a number of galaxies in the vicinity of the system (Figure 2, bottom left) that could have stripped gas from VCC 2034 (Table 1). To the SE of AGC 226178, VCC 2048 and VCC 2045 are at $cz_\odot = 1086$ and $1245\,\mathrm{km\,s^{-1}}$, respectively. Although neither of these can be entirely ruled out, if they are as close to VCC 2034 as they appear in projection and interacting with it, it would be puzzling why the H I features do not clearly extend toward them. Furthermore, they are separated from AGC 226178 by approximately 500 and $300\,\mathrm{km\,s^{-1}}$, respectively; thus, unless the encounter occurred at high speed (considered further below) with a large component of the relative velocity along the line of sight, neither of these are likely candidates.

Object VCC 2037 appears to be adjacent to VCC 2034 as if they are an interacting pair; indeed, the distribution of H I in VCC 2037 looks to be disturbed (Figure 2, bottom left). However, the two galaxies are separated by $\sim 350\,\mathrm{km\,s^{-1}}$ in velocity, and VCC 2037 has both TRGB and TFR distance estimates (Karachentsev et al. 2013, 2014) that place it well within the foreground of the Virgo cluster at about 10 Mpc. Therefore, this pair seems to be a chance projection (although VCC 2034 does not have a redshift-independent distance estimate). We also note that this implies that an additional, separate perturber is needed to explain the morphology of VCC 2037, as ram pressure cannot be the culprit in this case.

The other remaining candidate is NGVS 3543 itself. Although it seems an unlikely candidate for a perturber given its diffuse nature, it is right next to AGC 226178 and (assuming they are at the same distance) has a comparable stellar mass to VCC 2034 (Durbala et al. 2020; Junais et al. 2021); therefore, it should be considered. However, the fact that so many stars are identifiable in its CMD (Figure 1, top middle) suggests that it may be closer than Virgo. At the distance of Virgo, the TRGB would be expected to fall at approximately magnitude 27 (F814W). The CMD (Figure 1, top middle) shows many RGB stars brighter than this magnitude, and we therefore discount it as a potential perturber. A more detailed discussion of NGVS 3543 follows in the next subsection.

This leaves us with no strong candidate for the galaxy that perturbed VCC 2034. If both VCC 2034 and AGC 226178 are in Virgo, then it is possible that a high-speed encounter with another galaxy triggered the H I tail and the formation of AGC 226178, but that galaxy is now sufficiently far away that it is not an obvious candidate. In a cluster, the relative velocities of galaxies could be many hundreds of kilometers per second. As the radial velocity of AGC 226178 is so similar to VCC 2034 ($c\Delta z < 80\,\mathrm{km\,s^{-1}}$), it is reasonable to assume that the principal component of the velocity of the encounter would have been transverse to the line of sight. The oldest observed stars in AGC 226178 are probably $\sim 100\,\mathrm{Myr}$ old, and if we assume that the tidal interaction occurred a factor of a few times longer ago, then the perturber might be up to $1°$ away at present.

If we assume that the perturber is at the distance of Virgo and has a stellar mass equal to or greater than that of VCC 2034, then we can begin to narrow down the possibilities. We searched the SDSS spectrophotometric catalog (Strauss et al. 2002; Ahumada et al. 2020) for galaxies with redshifts less than $3000\,\mathrm{km\,s^{-1}}$. Using the Taylor et al. (2011) relation to estimate their stellar masses (based on the g- and i-band cModelMags and assuming $D = 16.5\,\mathrm{Mpc}$), we selected only those with $\log M_*/M_\odot > 8.2$, the estimated stellar mass of

VCC 2034 (Section 3.4). This narrows down the possible perturbers to seven objects: VCC 1948, VCC 2012, VCC 2042, VCC 2045, VCC 2048, VCC 2073, and VCC 2080. As only VCC 1948 and VCC 2048 have redshift-independent distance estimates, it is difficult to choose between these objects. But if we further restrict the velocity range to be within $\sim 100\,\mathrm{km\,s^{-1}}$ of AGC 226178 or VCC 2034, then VCC 1948 and VCC 2080 would appear to be the best candidates at $cz_\odot = 1610$ and $1532\,\mathrm{km\,s^{-1}}$, respectively. As VCC 2080 is to the NE, this would more naturally match the geometry of the system. However, even if this were the perturber, at $49'$ away, proving a definitive association may not be possible at this stage.

We therefore conclude that while a tidal interaction remains a definite possibility for the mechanism responsible for removing gas from VCC 2034 (and thereby forming AGC 226178), if this system is in the Virgo cluster (as the currently available evidence seems to imply), then there is no strong candidate for the would-be perturber, although there are multiple possible candidates.

An alternative explanation would be if both VCC 2034 and AGC 226178 were foreground objects at $\sim 10\,\mathrm{Mpc}$. In this case, VCC 2037 would presumably be interacting with VCC 2034 and a strong candidate for the perturber. There is another object, similar to AGC 226178, that is known to exist in the foreground of Virgo, namely, Coma P (also known as AGC 229385; Janowiecki et al. 2015; Ball et al. 2018). Coma P is the most massive of a system of three neighboring objects that are all detected in H I approximately $8°$ north of M87. Like AGC 226178, Coma P's stellar counterpart was first identified through its UV emission in GALEX and only later confirmed in the optical with deep imaging (Janowiecki et al. 2015). Although Coma P was originally assumed to be behind the Virgo cluster based on its radial velocity, a recent TRGB distance estimate (Brunker et al. 2019) revealed that Coma P is in fact much closer ($\sim 5.5\,\mathrm{Mpc}$), placing it in a relatively low-density foreground environment (however, see also Anand et al. 2018). This case demonstrates that objects similar in appearance to AGC 226178 could be foreground objects. However, as discussed in Section 4.1, a distance of 10 Mpc for AGC 226178 is strongly disfavored (though not ruled out) by the available data. Obtaining a direct distance estimate for VCC 2034 would be the most straightforward means to ruling out this possibility.

4.3. Distance to and Nature of NGVS 3543

Upon first inspection, the close proximity of AGC 226178 and NGVS 3543 might imply that the two objects are physically associated and at approximately the same distance. Using the CMD of NGVS 3543 (Figure 1, top middle), we attempted to measure the TRGB to obtain an accurate distance estimate. However, these measurements failed to reliably converge, likely owing to the paucity of stars and the proximity of the TRGB to the completeness limit. Instead, we turn to the observed luminosity function shown in Figure 4. This indicates that the TRGB likely occurs at F814W ≈ 26 (very close to the 90% completeness limit), which corresponds to a distance of $\sim 10\,\mathrm{Mpc}$. The stars brighter than this in the CMD likely belong to an asymptotic giant branch (AGB) population (analogous to the case in Sand et al. 2014). We also find that the distribution of these candidate AGB stars is considerably more compact than that of the candidate RGB stars, suggesting that they may
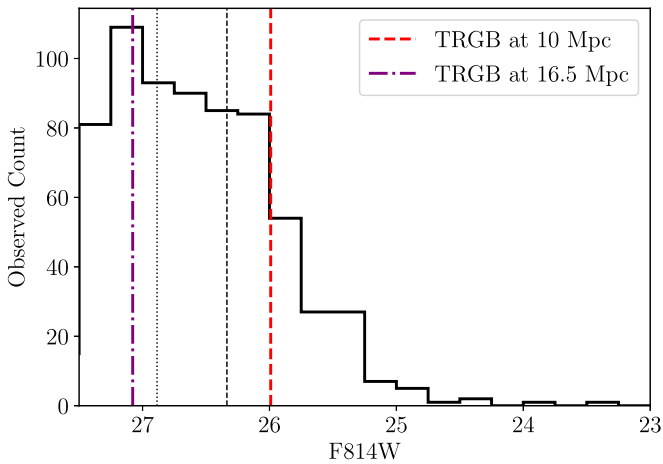
Figure 4. Observed luminosity function of stars in the NGVS 3543 CMD (Figure 1, top middle). The red dashed line indicates where the TRGB would occur (Jang & Lee 2017) for an RGB population with $F606W - F814W = 1$ and a fiducial distance of 10 Mpc, and the purple dashed–dotted line corresponds to if NGVS 3543 were at 16.5 Mpc (in Virgo), rather than 10 Mpc. The gray dashed line indicates the 90% completeness limit (at $F606W - F814W = 1$), and the gray dotted line is the 50% limit.

be a younger population. The CMD of NGVS 3543 can also be compared to another dwarf spheroidal known to be in the Virgo cluster, Dw J122147+132853 (Bellazzini et al. 2018, their Figure 6). The majority of the detected stars in this dwarf are fainter than $F814W = 27$, and there are almost no stars brighter than $F814W = 26$. This comparison reaffirms that NGVS 3543 is significantly nearer than the Virgo cluster.

Our distance estimate of $\sim$10 Mpc contradicts Junais et al. (2021), who assumed that AGC 226178 and NGVS 3543 were at the same distance (in the Virgo cluster) and physically interacting due to a faint bridge of UV emission between them (their Figure 1). However, with the HST imaging (and MUSE observations), it is clear that there is a clump of blue stars projected between the main body of AGC 226178 and NGVS 3543 (green dashed circle near the center of the left panel of Figure 1), which likely explains this apparent bridge of UV emission. Given that AGC 226178 is highly clumpy and irregular, this configuration could easily have occurred by chance.

Junais et al. (2021) also estimated the mass of NGVS 3543 (without a ram pressure stripping event) as $\log M_*/M_\odot = 7.31 \pm 0.27$ (if it were in Virgo), which, if it follows the MZR of Kirby et al. (2013), would mean it has $\langle[\text{Fe/H}]\rangle = -1.3 \pm 0.2$.[30] Assuming a solar ratio of Fe/O (Asplund et al. 2009), this equates to $12 + \log\text{O/H} \approx 7.4$. This value is almost an order of magnitude lower than that of AGC 226178 (Section 3.4), reinforcing that it is unlikely that the gas in AGC 226178 originated in NGVS 3543 (as hypothesized by Junais et al. 2021). Moving NGVS 3543 to 10 Mpc would reduce the stellar mass estimate of Junais et al. (2021) to $\log M_*/M_\odot = 6.88 \pm 0.27$, its absolute magnitude to $M_g = -12.5$, and its metallicity estimate to $\langle[\text{Fe/H}]\rangle = -1.4 \pm 0.2$, further exacerbating the discrepancy.

At a distance of $\sim$10 Mpc, it is likely that NGVS 3543 is associated with VCC 2037, approximately $12'$ (36 kpc) to the SW, which has a prior TRGB distance estimate of 9.6 Mpc (Karachentsev et al. 2014). Although at 10 Mpc, NGVS 3543

would not quite be classified as a UDG (as its half-light radius would be <1.3 kpc), it is similar in appearance. Tidal stripping is a promising mechanism for forming such galaxies (e.g., Bennet et al. 2018; Carleton et al. 2019; Jiang et al. 2019; Liao et al. 2019; Jones et al. 2021); thus, its association with VCC 2037 might explain its appearance. Furthermore, it is possible that an interaction with VCC 2037 led to the recent quenching of this object that Junais et al. (2021) proposed. Alternatively, NGVS 3543 may simply be a field dwarf at a slightly different distance to VCC 2037. However, if this were the case, it would be an exceptionally odd system, as it has a diffuse morphology and UV emission but no detectable H I, and its CMD is dominated by red stars.

4.4. Fate of AGC 226178

The position of the stars in the CMD of AGC 226178 (Figure 1, bottom right) indicates that there is likely some spread in their ages in the approximate range 10–100 Myr. This would also be consistent with the close agreement in the SFR estimates from NUV and FUV, suggesting that the SFR has been somewhat constant on the order of 100 Myr. Furthermore, a sustained SFR of $\sim 10^{-3}\,M_\odot\,\text{yr}^{-1}$ (Section 3.2) over 100 Myr would produce a total stellar mass of $\sim 10^5\,M_\odot$, similar to the stellar mass estimate of Junais et al. (2021), $5 \times 10^4\,M_\odot$. At its present SFR, AGC 226178 could go on producing stars for several Hubble times without running out of gas. However, it is unlikely that it will be able to retain its gas on a long (>1 Gyr) timescale.

As it appears to have formed from stripped material, AGC 226178 is unlikely to contain a significant quantity of dark matter, and as its total baryonic mass is less than $10^8\,M_\odot$, it does not meet the threshold typically assumed for a TD to be long-lived (Bournaud & Duc 2006). This means that AGC 226178 is unlikely to be self-gravitating, and even if it is, it is unlikely to remain so on a gigayear timescale. Therefore, it may not be appropriate to refer to it as a galaxy (Willman & Strader 2012), and we have tried to avoid doing so. However, unlike in field and group environments, where TDs are typically studied, it has been suggested that the hot ICM may actually assist low-mass, gas-rich objects in remaining bound longer than would be expected from their internal gravity alone, as this can add an additional external compression to the gas (Burkhart & Loeb 2016).

The fate of the H I component of a very similar object (SECCO 1) was investigated in detail by Bellazzini et al. (2018) and Calura et al. (2020). These works performed a series of high-resolution hydrodynamical simulations of a $10^7\,M_\odot$ gas cloud moving at up to $400\,\text{km s}^{-1}$ through a hot medium, finding that a significant fraction of its initial H I content could persist for on the order of 1 Gyr. However, instabilities in the gas cloud build up as it moves through the hot ICM, and on longer timescales, it will be broken up into smaller clouds and evaporate. As H I makes up the vast majority of the baryonic mass of AGC 226178 and provides the medium for external pressure equilibrium, once the H I is lost, it will almost certainly be unbound.

Given its low stellar mass, AGC 226178 is only visible at all in the optical because of its young, bright, blue stars. Once SF ceases, it will rapidly fade. After 100 Myr, only a handful of stars will be above the 90% completeness limit of our HST observations, and after 500 Myr, almost no individual stars will be detectable at all. Assuming its total stellar mass has not

---

[30] Here we do not use the relation from Andrews & Martini (2013), as NGVS 3543 is below the mass range covered by their sample.

dramatically increased in the intervening time (such that its integrated light would be detectable), it will become, for all intents and purposes, invisible (cf. Román et al. 2021), and its aging stars will become part of the intracluster light of Virgo.

4.5. A Larger Population of Blue Stellar Systems in Virgo

As alluded to by Sand et al. (2017), SECCO 1 and AGC 226178 are not the only objects of their kind. Both were originally identified by their H I emission in the ALFALFA survey and were noteworthy due to their near-invisible (in SDSS images) stellar counterparts. As part of this work, AGC 226178 was reidentified (independent of its original H I detection) during a visual search for faint, blue, and UV-emitting objects in the Virgo cluster using $\sim$100 deg^2 of publicly available NGVS images and GALEX tiles. A full analysis of this search will be presented in a subsequent paper (Jones et al. in preparation), but at least three additional objects were identified with very similar optical and UV properties to AGC 226178. Assuming that the other objects are also in Virgo and extremely young (as AGC 226178 appears to be), it is reasonable to assume that such objects are being continually created in the Virgo cluster. At present, these $\sim$five objects are known, and, based on the discussion above, each one may only be visible for $\sim$500 Myr. Therefore, these objects must be being produced in Virgo at a rate of $\sim$one per 100 Myr. However, it remains to be seen whether these form a uniform population with related formation mechanisms or are really a mixture of many different types of objects that happen to have similar appearances in the optical and UV.

5. Conclusions

The AGC 226178 and NGVS 3543 system is a disparate (false) pair of dwarf galaxies in the direction of the Virgo cluster, where foreground and background objects are frequently projected next to each other. With a reanalysis of ALFALFA and VLA data (Figures 2 and 3), we have demonstrated that AGC 226178 likely formed from gas stripped from VCC 2034, and that it is neither a normal gas-rich dwarf (Cannon et al. 2015) nor a stellar system formed through the ram pressure stripping of a UDG (Junais et al. 2021). The hypothesis is also supported by its high metallicity, indicating that its gas originated in a galaxy with a much higher stellar mass. Its apparent neighbor, NGVS 3543, appears to be a foreground object at approximately 10 Mpc, based on its CMD (Figures 1 and 4). At this distance, it would be too small to meet the classification criteria of a UDG.

The magnitude of the youngest, brightest stars in AGC 226178 is consistent with this object being in the Virgo cluster, though a direct distance measurement to either AGC 226178 or VCC 2034 would solidify this assessment. As both NGVS 3543 and VCC 2037 are foreground objects, there is no obvious candidate for the perturbing galaxy that stripped gas from VCC 2034 to form AGC 226178. This leaves two possible scenarios: (1) a high-speed close encounter with the perturber, now as much as a degree away, or (2) ram pressure stripping with VCC 2034 falling into Virgo with a large transverse velocity ($\sim$350 km s^{-1}).

Objects AGC 226178 and SECCO 1 are part of a larger sample of similar objects (e.g., Sand et al. 2017) in or observed toward Virgo that are similar in optical appearance and that we will present in an upcoming paper. These objects may really be a mixed collection of objects with differing formation mechanisms or may all have formed recently from stripped gas, like AGC 226178. Over the next several hundred mega-years, AGC 226178 (and other objects like it) will lose its neutral gas, stop forming stars, and fade from view, eventually becoming essentially invisible. Thus, for these objects to be visible at any given time, they must be being continually produced in the cluster.

Our findings highlight the complexity of studying systems in the direction of Virgo. In this field, there appear to be three close pairs (AGC 226178/NGVS 3543, VCC 2034/2037, and VCC 2045/2048), yet neither of the first two are genuine pairs. Instead, AGC 226178/VCC 2034 and NGVS 3543/VCC 2037 both form wide pairs ($\sim$15$'$ separation), but their members are projected into the two different, false, close pairs indicated above. In addition, both VCC 2034 and VCC 2037 have disturbed morphologies but do not appear to be interacting with each other, while the actual perturber of VCC 2034 is not evident. AGC 226178 itself is a peculiar "Almost Dark" system (comparable to SECCO 1) and immediately adjacent to it, but at a completely different distance, is a highly unusual dwarf spheroidal (NGVS 3543). We thus emphasize caution when interpreting these systems and the importance of exhaustive follow-up observations to eliminate possible interpretations.

Facilities: Arecibo, Blanco, GALEX, HST (ACS), VLA, VLT:Yepun (MUSE).

Software: DOLPHOT (Dolphin 2000), CASA (McMullin et al. 2007), astropy (Astropy Collaboration et al. 2013, 2018), APLpy (Robitaille & Bressert 2012; Robitaille 2019), Photutils (Bradley et al. 2020), reproject (Robitaille et al. 2020), DS9 (Joye & Mandel 2003), dustmaps (Green 2018), Astroalign (Beroiz et al. 2020), SExtractor (Bertin & Arnouts 1996), Aladin (Bonnarel et al. 2000; Boch & Fernique 2014).

ORCID iDs

Michael G. Jones ⓘ https://orcid.org/0000-0002-5434-4904
David J. Sand ⓘ https://orcid.org/0000-0003-4102-380X
Michele Bellazzini ⓘ https://orcid.org/0000-0001-8200-810X
Kristine Spekkens ⓘ https://orcid.org/0000-0002-0956-7949
John M. Cannon ⓘ https://orcid.org/0000-0002-1821-7019
Burçin Mutlu-Pakdil ⓘ https://orcid.org/0000-0001-9649-4815
Ananthan Karunakaran ⓘ https://orcid.org/0000-0001-8855-3635
Giacomo Beccari ⓘ https://orcid.org/0000-0002-3865-9906
Laura Magrini ⓘ https://orcid.org/0000-0003-4486-6802
Giovanni Cresci ⓘ https://orcid.org/0000-0002-5281-1417
John L. Inoue ⓘ https://orcid.org/0000-0002-9724-8998
Jackson Fuson ⓘ https://orcid.org/0000-0002-8598-439X
Elizabeth A. K. Adams ⓘ https://orcid.org/0000-0002-9798-5111
Giuseppina Battaglia ⓘ https://orcid.org/0000-0002-6551-4294
Paul Bennet ⓘ https://orcid.org/0000-0001-8354-7279
Denija Crnojević ⓘ https://orcid.org/0000-0002-1763-4128
Nelson Caldwell ⓘ https://orcid.org/0000-0003-2352-3202
Puragra Guhathakurta ⓘ https://orcid.org/0000-0001-8867-4234
Martha P. Haynes ⓘ https://orcid.org/0000-0001-5334-5166
Ricardo R. Muñoz ⓘ https://orcid.org/0000-0002-0810-5558
Anil Seth ⓘ https://orcid.org/0000-0003-0248-5470
Jay Strader ⓘ https://orcid.org/0000-0002-1468-9668
Elisa Toloba ⓘ https://orcid.org/0000-0001-6443-5570
Dennis Zaritsky ⓘ https://orcid.org/0000-0002-5177-727X

References

Adams, E. A. K., Giovanelli, R., & Haynes, M. P. 2013, ApJ, 768, 77
Adams, E. A. K., Oosterloo, T. A., Cannon, J. M., Giovanelli, R., & Haynes, M. P. 2016, A&A, 596, A117
Adams, E. A. K., Cannon, J. M., Rhode, K. L., et al. 2015, A&A, 580, A134
Ahumada, R., Prieto, C. A., Almeida, A., et al. 2020, ApJS, 249, 3
Anand, G. S., Tully, R. B., Karachentsev, I. D., et al. 2018, ApJL, 861, L6
Andrews, B. H., & Martini, P. 2013, ApJ, 765, 140
Asplund, M., Grevesse, N., Sauval, A. J., & Scott, P. 2009, ARA&A, 47, 481
Astropy Collaboration, Robitaille, T. P., Tollerud, E. J., et al. 2013, A&A, 558, A33
Astropy Collaboration, Price-Whelan, A. M., Sipőcz, B. M., et al. 2018, AJ, 156, 123
Bacon, R., Vernet, J., Borisova, E., et al. 2014, Msngr, 157, 13
Ball, C., Cannon, J. M., Leisman, L., et al. 2018, AJ, 155, 65
Beccari, G., Bellazzini, M., Battaglia, G., et al. 2016, A&A, 591, A56
Beccari, G., Bellazzini, M., Magrini, L., et al. 2017, MNRAS, 465, 2189
Bellazzini, M., Beccari, G., Battaglia, G., et al. 2015a, A&A, 575, A126
Bellazzini, M., Magrini, L., Mucciarelli, A., et al. 2015b, ApJL, 800, L15
Bellazzini, M., Armillotta, L., Perina, S., et al. 2018, MNRAS, 476, 4565
Bennet, P., Sand, D. J., Zaritsky, D., et al. 2018, ApJL, 866, L11
Beroiz, M., Cabral, J., & Sanchez, B. 2020, A&C, 32, 100384
Bertin, E., & Arnouts, S. 1996, A&AS, 117, 393
Boch, T., & Fernique, P. 2014, in ASP Conf. Ser., 485, Astronomical Data Analysis Software and Systems XXIII, ed. N. Manset & P. Forshay (San Francisco, CA: ASP), 277
Bonnarel, F., Fernique, P., Bienaymé, O., et al. 2000, A&AS, 143, 33
Boselli, A., Boissier, S., Heinis, S., et al. 2011, A&A, 528, A107
Boselli, A., Fossati, M., Ferrarese, L., et al. 2018, A&A, 614, A56
Bournaud, F., & Duc, P. A. 2006, A&A, 456, 481
Bradley, L., Sipőcz, B., Robitaille, T., et al. 2020, astropy/photutils: 1.0.0, Zenodo, doi:10.5281/zenodo.4044744
Bressan, A., Marigo, P., Girardi, L., et al. 2012, MNRAS, 427, 127
Brunker, S. W., McQuinn, K. B. W., Salzer, J. J., et al. 2019, AJ, 157, 76
Burkhart, B., & Loeb, A. 2016, ApJL, 824, L7
Calura, F., Bellazzini, M., & D'Ercole, A. 2020, MNRAS, 499, 5873
Cannon, J. M., Martinkus, C. P., Leisman, L., et al. 2015, AJ, 149, 72
Carleton, T., Errani, R., Cooper, M., et al. 2019, MNRAS, 485, 382
Chung, A., van Gorkom, J. H., Kenney, J. D. P., Crowl, H., & Vollmer, B. 2009, AJ, 138, 1741
Cramer, W. J., Kenney, J. D. P., Sun, M., et al. 2019, ApJ, 870, 63
Dalessandro, E., Schiavon, R. P., Rood, R. T., et al. 2012, AJ, 144, 126
Dey, A., Schlegel, D. J., Lang, D., et al. 2019, AJ, 157, 168
Dolphin, A. 2016, DOLPHOT: Stellar Photometry, Astrophysics Source Code Library, ascl:1608.013
Dolphin, A. E. 2000, PASP, 112, 1383
Durbala, A., Finn, R. A., Crone Odekon, M., et al. 2020, AJ, 160, 271
Ferrarese, L., Côté, P., Cuillandre, J.-C., et al. 2012, ApJS, 200, 4
Giovanelli, R., Haynes, M. P., Kent, B. R., et al. 2005, AJ, 130, 2598
Giovanelli, R., Haynes, M. P., Adams, E. A. K., et al. 2013, AJ, 146, 15
Goudfrooij, P. 2018, ApJ, 857, 16
Green, G. M. 2018, JOSS, 3, 695
Haynes, M. P., Giovanelli, R., Martin, A. M., et al. 2011, AJ, 142, 170
Haynes, M. P., Giovanelli, R., Kent, B. R., et al. 2018, ApJ, 861, 49
Hibbard, J. E., van Gorkom, J. H., Rupen, M. P., & Schiminovich, D. 2001, in ASP Conf. Ser., 240, Gas and Galaxy Evolution, ed. J. E. Hibbard, M. Rupen, & J. H. van Gorkom (San Francisco, CA: ASP), 657
Huang, S., Haynes, M. P., Giovanelli, R., & Brinchmann, J. 2012, ApJ, 756, 113
Iglesias-Páramo, J., Buat, V., Takeuchi, T. T., et al. 2006, ApJS, 164, 38
Irwin, M. J., Belokurov, V., Evans, N. W., et al. 2007, ApJL, 656, L13
Jang, I. S., & Lee, M. G. 2017, ApJ, 835, 28
Janowiecki, S., Leisman, L., Józsa, G., et al. 2015, ApJ, 801, 96
Jiang, F., Dekel, A., Freundlich, J., et al. 2019, MNRAS, 487, 5272
Jones, M. G., Bennet, P., Mutlu-Pakdil, B., et al. 2021, ApJ, 919, 72
Joye, W. A., & Mandel, E. 2003, in ASP Conf. Ser., 295, Astronomical Data Analysis Software and Systems XII, ed. H. E. Payne, R. I. Jedrzejewski, & R. N. Hook (San Francisco, CA: ASP), 489
Junais, Boissier, S., Boselli, A., et al. 2021, A&A, 650, A99
Karachentsev, I. D., Makarov, D. I., & Kaisina, E. I. 2013, AJ, 145, 101
Karachentsev, I. D., Tully, R. B., Wu, P.-F., Shaya, E. J., & Dolphin, A. E. 2014, ApJ, 782, 4
Kennicutt, R. C. J. 1998, ARA&A, 36, 189
Kent, B. R., Giovanelli, R., Haynes, M. P., et al. 2008, AJ, 136, 713

Kewley, L. J., Dopita, M. A., Sutherland, R. S., Heisler, C. A., & Trevena, J. 2001, ApJ, 556, 121

Kim, S., Rey, S.-C., Jerjen, H., et al. 2014, ApJS, 215, 22

Kirby, E. N., Cohen, J. G., Guhathakurta, P., et al. 2013, ApJ, 779, 102

Kniazev, A. Y., Pustilnik, S. A., & Zucker, D. B. 2008, MNRAS, 384, 1045

Liao, S., Gao, L., Frenk, C. S., et al. 2019, MNRAS, 490, 5182

Martin, D. C., Fanson, J., Schiminovich, D., et al. 2005, ApJL, 619, L1

Martin, N. F., Weisz, D. R., Albers, S. M., et al. 2017, ApJ, 850, 16

Masters, K. L. 2005, PhD thesis, Cornell University, New York, USA

McMullin, J. P., Waters, B., Schiebel, D., Young, W., & Golap, K. 2007, in ASP Conf. Ser., 376, Astronomical Data Analysis Software and Systems XVI, ed. R. A. Shaw, F. Hill, & D. J. Bell (San Francisco, CA: ASP), 127

McQuinn, K. B. W., Skillman, E. D., Dalcanton, J. J., et al. 2011, ApJ, 740, 48

Mei, S., Blakeslee, J. P., Côté, P., et al. 2007, ApJ, 655, 144

Minchin, R. F., Taylor, R., Köppen, J., et al. 2019, AJ, 158, 121

Monaco, L., Bellazzini, M., Ferraro, F. R., & Pancino, E. 2003, ApJL, 597, L25

Morrissey, P., Conrow, T., Barlow, T. A., et al. 2007, ApJS, 173, 682

Perina, S., Bellazzini, M., Buzzoni, A., et al. 2012, A&A, 546, A31

Pettini, M., & Pagel, B. E. J. 2004, MNRAS, 348, L59

Rizzi, L., Tully, R. B., Makarov, D., et al. 2007, ApJ, 661, 815

Robitaille, T. 2019, APLpy v2.0: The Astronomical Plotting Library in Python, doi:10.5281/zenodo.2567476

Robitaille, T., & Bressert, E. 2012, APLpy: Astronomical Plotting Library in Python, Astrophysics Source Code Library, ascl:1208.017

Robitaille, T., Deil, C., & Ginsburg, A. 2020, reproject: Python-based astronomical image reprojection, Astrophysics Source Code Library, ascl:2011.023

Román, J., Jones, M. G., Montes, M., et al. 2021, A&A, 649, L14

Sand, D. J., Crnojević, D., Strader, J., et al. 2014, ApJL, 793, L7

Sand, D. J., Crnojević, D., Bennet, P., et al. 2015, ApJ, 806, 95

Sand, D. J., Seth, A. C., Crnojević, D., et al. 2017, ApJ, 843, 134

Saul, D. R., Peek, J. E. G., Grcevich, J., et al. 2012, ApJ, 758, 44

Schlafly, E. F., & Finkbeiner, D. P. 2011, ApJ, 737, 103

Schlegel, D. J., Finkbeiner, D. P., & Davis, M. 1998, ApJ, 500, 525

Serra, P., Westmeier, T., Giese, N., et al. 2014, SoFiA: Source Finding Application, Astrophysics Source Code Library, ascl:1412.001

Serra, P., Westmeier, T., Giese, N., et al. 2015, MNRAS, 448, 1922

Strauss, M. A., Weinberg, D. H., Lupton, R. H., et al. 2002, AJ, 124, 1810

Taylor, E. N., Hopkins, A. M., Baldry, I. K., et al. 2011, MNRAS, 418, 1587

Taylor, R., Köppen, J., Jáchym, P., et al. 2020, AJ, 159, 218

Theureau, G., Hanski, M. O., Coudreau, N., Hallet, N., & Martin, J. M. 2007, A&A, 465, 71

van Dokkum, P. G., Abraham, R., Merritt, A., et al. 2015, ApJL, 798, L45

Villegas, D., Jordán, A., Peng, E. W., et al. 2010, ApJ, 717, 603

Willman, B., & Strader, J. 2012, AJ, 144, 76

Wyder, T. K., Martin, D. C., Schiminovich, D., et al. 2007, ApJS, 173, 293

Yoon, S.-J., Lee, Y.-W., Rey, S.-C., Ree, C. H., & Yi, S. K. 2004, Ap&SS, 291, 223

York, D. G., Adelman, J., Anderson, J. E. J., et al. 2000, AJ, 120, 1579